Available online at www.sciencedirect.com

jmr&t Journal of Materials Research and Technology

https://www.journals.elsevier.com/journal-of-materials-research-and-technology

Original Article

Comparative study of nanostructured titania grown by electrochemical anodization of α-Ti and β-TiNi substrates in organic electrolytes

Pedro Damas Resende, Rosa Maria Rabelo Junqueira, Jéssica Dornelas Silva, Natália Isabel Azevedo Lopes, Leandro Arruda Santos, Vicente Tadeu Lopes Buono*

Department of Metallurgical and Materials Engineering, Universidade Federal de Minas (UFMG), Belo Horizonte, Minas Gerais, Brazil

ARTICLE INFO

Article history:
Received 13 April 2020
Accepted 5 July 2020
Available online 26 July 2020

Keywords:
Nickel-Titanium
Anodization
Titania nanotubes
Anodic films
Nanostructured oxide films

ABSTRACT

The motivation of this work is to compare methods for nanotube formation in α-Ti with the results obtained in β-TiNi by electrochemical anodization at the same conditions. Both substrates were characterized by XRD to assure their phase constitution at room temperature. Samples were anodized in 0.2%m. NH_4F and 1%v. H_2O in ethylene glycol solvent at 5, 15, 25, 45, and 60 V. Each experimental condition had its current densities recorded as a function of time and the resultant anodic films were characterized by FE-SEM. All conditions lead to nanotube formation in Ti substrates. TiNi samples anodized at 5 V produced evenly spread nanotubes with similar diameters of those in Ti. As the potential increased, the nanotubular aspects of titania in TiNi were increasingly lost. At higher anodization potentials, tubular structures can be seen in a matrix of sponge-like oxide formed due to the increase of oxygen evolution as the potential increased. Examination of the metal/oxide interface indicates that, even though spongy oxide was formed in TiNi substrates, the mechanism of growth initiation is similar to Ti samples. It is possible to conclude that for the same anodization conditions β-TiNi is more reactive than α-Ti and requires milder conditions to produce nanotubular surfaces.

1. Introduction

Titanium and titanium alloys are widely used in many fields because of their intrinsic properties such as low elastic modulus, high biocompatibility, high corrosion resistance, and high strength to weight ratio [1,2]. In some devices, the metal surfaces can be tailored to enhance their performance in the proposed use by different means. Anodization is presented as a relatively easy and cost-effective way to obtain desired nanostructured surfaces in metals and alloys by changing process variables. Among diverse titania nanostructures, nanotube (NT) arrays obtained by electrochemical anodization arise as a sound method to functionalize surfaces because of its unique properties and potential uses for biomedical [3–5],

* *Corresponding author.*
E-mail: pedrodamas0803@ufmg.br (P.D. Resende).

https://doi.org/10.1016/j.jmrt.2020.07.009

energy harvesting [6–8], photocatalysis [9] and sensing [10] applications.

Titania nanotubes (TNT's) on commercially pure titanium (cp-Ti) were firstly mentioned by Gong et al. [11] and were obtained by electrochemical anodization in 0.2%wt. HF aqueous electrolytes at a constant potential of 20 V for 20 min. The work of Gong et al. was proposed after Zwilling et al. [12] found hollow elongated structures growing normally to the substrate on the anodization of Ti and Ti6Al4V in a mixed electrolyte of CA (chromic acid) and HF. Since then, researchers have put a lot of effort to gain comprehension of the specific phenomena involved in the growth of such nanostructures. The methods for NT's growth can be divided into three generations characterized by differences in electrolyte types [13,14]. The first generation is based on the anodization of Ti in HF based aqueous solutions as proposed by Gong et al. [11]. Changes have been made upon the second generation as researchers have found that pH plays an important role in the smoothness of TNT's and its length. Saline based electrolytes and non-acidic fluoride sources were proposed to increase the pH of anodization processes and took NT's thickness from nanometer to micrometer scale. The third generation of TNT's can achieve hundreds of micrometers in thickness and is characterized by anodizing Ti in organic electrolytes, most common are ethylene glycol and glycerol, with additions of 1–5%v. H_2O and 0.1 - 0.5%wt. NH_4F [13].

TNTs' morphology is directly affected by different anodization parameters and the most relevant are the applied potential and time. But it is important to highlight that base metal chemical and phase composition [15], previous surface condition [16], pressure [17,18], temperature [19], light incidence [18] can also affect NTs morphology. The time is directly associated with the thickness of the grown anodic film, longer anodization times leading to thicker films [20]. This statement is true up to a critical value when the growth rate and dissolution of the TiO_2 rate by fluoride reach a steady-state and thickness can no longer grow [21]. The potential has a strong correlation with pore diameter, which increases as the potential is increased [22].

The majority of the studies aiming to produce titania NTs are based on the anodization of α-Ti substrate, usually of commercial-grade Ti. Few research deals with the anodization of α/β Ti-based alloys, commonly used for biomedical applications [12,15,23,24]. Zwilling and co-workers [12] found that nanotubular anodic films produced on top of the β phase of Ti6Al4V have different pore size distribution compared to what is obtained over α phase and are deeper than its surroundings, suggesting a more rapid chemical attack of the β phase during anodization. Lee et al. [15] studied the anodization of Ti, Ti-Ta, and Ti6Al4V alloys and their results pointed to the fact that multi-constituted alloy microstructure originates TNT's with different degrees of organization. They also have found that the β phase of Ti6Al4V produces a sponge-like oxide morphology whilst the α phase grows well-organized TNT's. Matykina et al. [23] found that the β phase is completely dissolved during the anodization process and anodic oxidation proceeds over the underlying α phase of Ti6Al4V, evidence supported by Moravec et al. [24].

Approximately equiatomic TiNi alloys are constituted by the β phase structure and present superelasticity or shape memory effect, key factors to their usage. These properties are related to a reversible martensitic transformation [25] from the β phase. Even though the anodic processing of cp-Ti and its α alloys to achieve nanotubular titania structured surfaces is broadly explored in the literature, that is not the case of fully β titanium-based alloys, especially for the Ti-Ni system. Anodization of TiNi alloys aiming to obtain TNT's is a relatively scarce and not well-established field of research reported on the available literature [26–29]. The lack of directives and knowledge on how the existent Ti anodization information can be applied to TiNi alloy and to what extent the results would be different due to the substrate change is the motivation of the present work. Therefore, the objective of the present study is to compare differences in the results of nanostructured films obtained by anodization of cp-Ti and TiNi under the same conditions.

2. Experimental procedures

Strips of commercially pure titanium and TiNi of nominal composition 50,8%at. Ni were used to perform electrochemical anodization and further characterization. The samples were cleaned in a two-step degreasing process, initially in ethanol and then in acetone, under sonication for 30 min.

2.1. *Substrate characterization*

Both substrates were characterized by X-Ray diffraction (XRD; *Panalytical PW1710, Almelo, The Netherlands*) operating with Cu kα (λ =0.15418 nm) using a scan rate of 0.02°/s at room temperature (RT). The phases were identified by comparison with patterns available at *Inorganic Crystal Structure Database* (ICSD, Code#43416 for Ti and Code#166366 for TiNi).

Due to the reversibility nature of martensitic transformations in the TiNi alloy as a function of temperature, differential scanning calorimetry (DSC; *DSC60, Shimadzu, Tokyo, Japan*) was used to characterize phase transition temperatures for TiNi samples and to assure that at anodization conditions only the β phase was present. Samples were heated up to 100 °C starting at -100 °C and then cooled again to -100 °C at heating/cooling rates of 10 °C/min. Transition temperatures were determined by intersecting baseline and a tangent at the onset of transformation peaks.

2.2. *Electrochemical anodization*

Anodization was carried out on a two-electrode electrochemical cell with a constant voltage supply (Keithley 2260B, *Cleveland, USA*). The electrolyte composition was 0.2 %wt. NH_4F, 1%v. H_2O in ethylene glycol, and was chosen based on a literature survey for TNT's growth on TiNi substrates [26,28,30]. The Ti cathode with an area of 4 cm^2 was placed 2 cm apart from the anode and had approximately twice the surface area of the anode. Samples of Ti and TiNi were anodized under voltages of 5, 15, 25, 45, and 60 V in approximately 50 mL of electrolyte without stirring. The total anodization time was 3 h for all the experimental conditions. Some anodization conditions were replicated with different total time if it was found necessary to assess morphological features of anodic film at

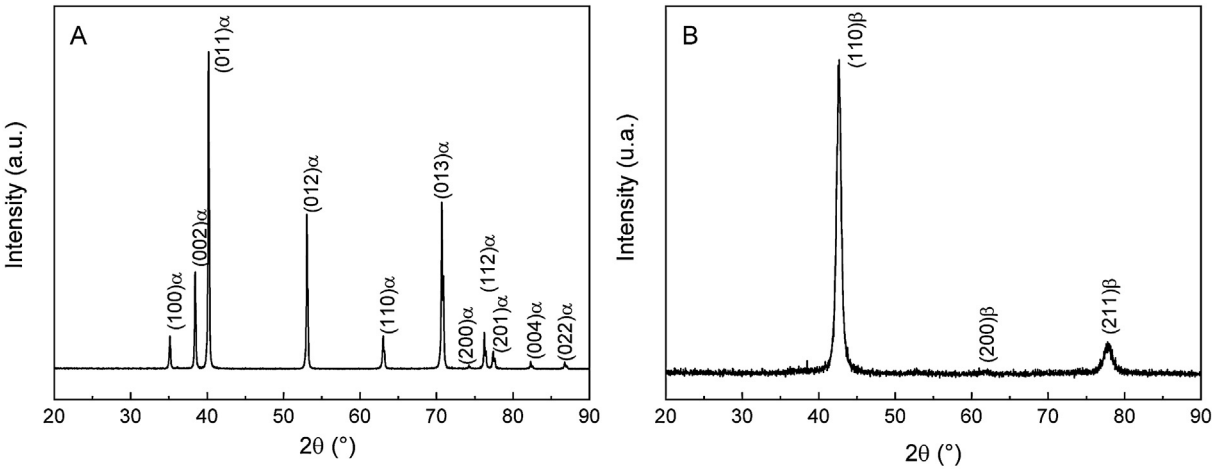

Fig. 1 – X-Ray diffraction patterns of (A) cp-Ti and (B) TiNi.

these conditions. Total anodization current was measured with a digital ammeter (Tektronix DMM4020, *Beaverton, USA*) and plotted as a function of time. After anodization, all samples were immediately washed with distilled water, rinsed in ethanol for 30 min and then dried in N_2 dry gas stream.

2.3. *Anodic film characterization*

Anodic film top surfaces were observed under field emission scanning electronic microscopy (FE-SEM, FEI Quanta 3D) using an acceleration potential of 5 kV and secondary electron imaging. Qualitative composition data was obtained using energy dispersive spectroscopy (EDS). Nanotube diameters were measured using free software ImageJ 1.52q (National Institute of Health, USA) [31]. At least 50 measurements per sample were performed and the results were statistically analyzed with R version 3.5.2 [32] at a level of significance of 0.05. Results were compared using a two-way analysis of variance to determine the influence of substrate type and anodization potential on the film characteristics. Tukey's honestly significant difference (Tukey's HSD) post hoc test was used to compare pairwise differences amongst groups. For further analysis of the self-organization of anodic film, samples anodized at 25 V were glued to carbon conductive tape and the film was detached to observe its bottom part under FE-SEM.

3. Results and discussion

The X-Ray diffraction patterns of both substrates are shown in Fig. 1. Results for cp-Ti (Fig. 1A), indexed according to pattern code #43416, show that the material is monophasic with all reflections matching the α-Ti phase. The same behavior is observed in Fig. 1(B) for the TiNi sample after comparison with pattern code #166366, except for the fact that some peaks in the analyzed range are absent for β-TiNi. This, together with a prominent peak broadening, is an indication that the material has small grain size and/or lattice defects accumulation due to cold work followed by low-temperature annealing [25]. DSC results show that the austenite finish temperature of the TiNi alloy is Af = 18.5 °C. The Af temperature depends on the chemical composition of the alloy and its thermomechanical processing history and is the temperature above which the alloy is fully β constituted [25]. Thus, the DSC results confirm that at the anodization conditions the TiNi alloy is fully β.

The total anodization current was measured as a function of time and the results are presented in Fig. 2. The current density curves of both materials show that a higher anodization potential leads to higher current densities during anodization. When the same anodization potential is compared for both materials, it can be noticed that TiNi related current densities tend to be higher along the electrochemical process. All anodization conditions of Ti produced nanotubular structures, as shown in Fig. 3.

According to field-assisted dissolution equilibrium theory (FADET), *i x t* curves of anodization aiming to produce titania nanotubes on Ti and its alloys can be divided into three stages closely related to morphological changes of the anodic film as anodization time increases. The first stage is associated with barrier oxide thickening and the current density drops exponentially until the second stage is reached. The second part of the curve starts at the moment that current density rises due to the pore growth initiation and its intrinsic specific area increase. After pore initiation, a steady state is reached and the pores grow at a constant current until the end of the process is achieved [33]. However, recent studies have shown strong evidence against FADET because of its lack of consistency in the explanation of pore initiation and the auto-organization phenomena itself [13]. Electronic current theory states that the mechanism of pore initiation and growth relies on the presence of sufficiently high electronic current to induce gaseous oxygen evolution at the interface of anion contaminated layer and the barrier oxide layer. As oxygen bubbles are formed and grow, its internal pressure rises acting as a mold where oxide grows around [34]. Oxide formation is related to the ionic component of total anodizing current and its growth around the oxygen bubble mold is enhanced by electrostriction forces [34–37].

The presence of an alloying element in TiNi alloy adds another level of complexity to the current density curve of anodization. In natural conditions of surface passivation, TiO_2

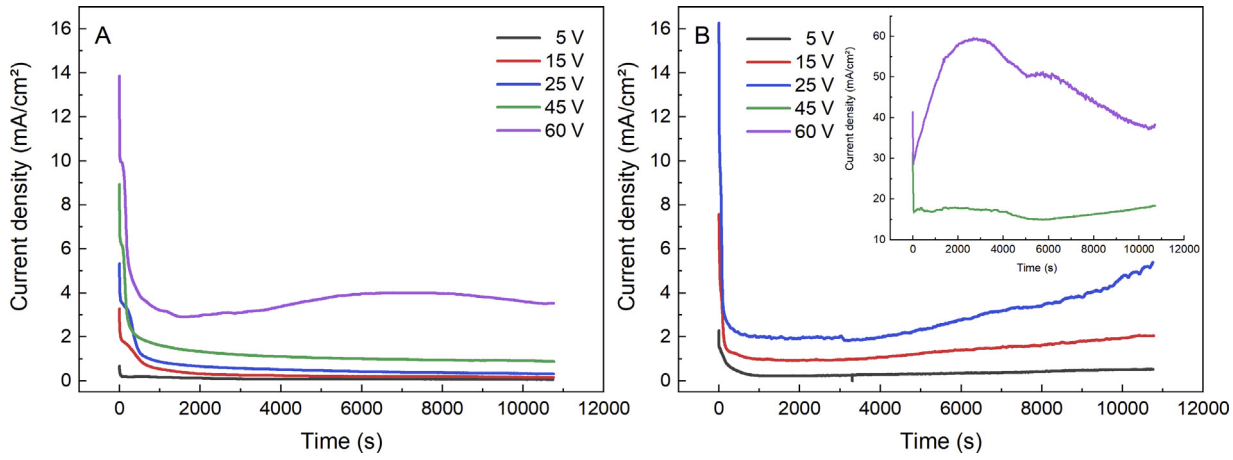

Fig. 2 – Current density x time curves of (A) cp-Ti and (B) NiTi at different anodization potentials. NiTi anodization curves at 45 and 60 V are presented in the (B) inset.

is preferentially produced instead of the other viable oxidation phases due to thermodynamic aspects of the involved chemical reactions [38]. However, when the oxidation of TiNi surfaces occurs under anodization conditions, the high electrical field induces ionic mobility of nickel atoms that contribute to the measured current density in the anodization process. Hang et al. [30] measured an atomic ratio of Ni/Ti around 0.25 with XPS in anodic films processed in similar conditions and attributed the lower content of Ni to its higher complexation rate with free F- ions in the electrolyte. Thus, the ionic component of the current density of TiNi samples involves the transport of Ni, Ti, and O ions, whilst for cp-Ti, only Ti and O species are involved. The EDS analysis shows that after anodization O is present at the surface of the samples together with residual F and C. According to the electronic current and bubble mold theory, the electronic current makes the total current density higher due to gaseous oxygen evolution at the anion contaminated and barrier oxide layers interface [35–37]. On the other hand, the ionic current drops exponentially since the beginning of the process and tends to stabilize as the transport rate of metal and oxygen ions in opposite directions reaches equilibrium. These current components together form the typical shape of an *i* x *t* curve. In our results, similar behavior was found only for Ti anodization at 60 V in Fig. 2(A). This experimental group has abnormally higher top tube diameter when compared to the other conditions as shown in Fig. 3, suggesting that even though nanotubular structures were produced for lower potentials, the electronic current component was too low for the precision of used ammeter and, therefore, the magnitude

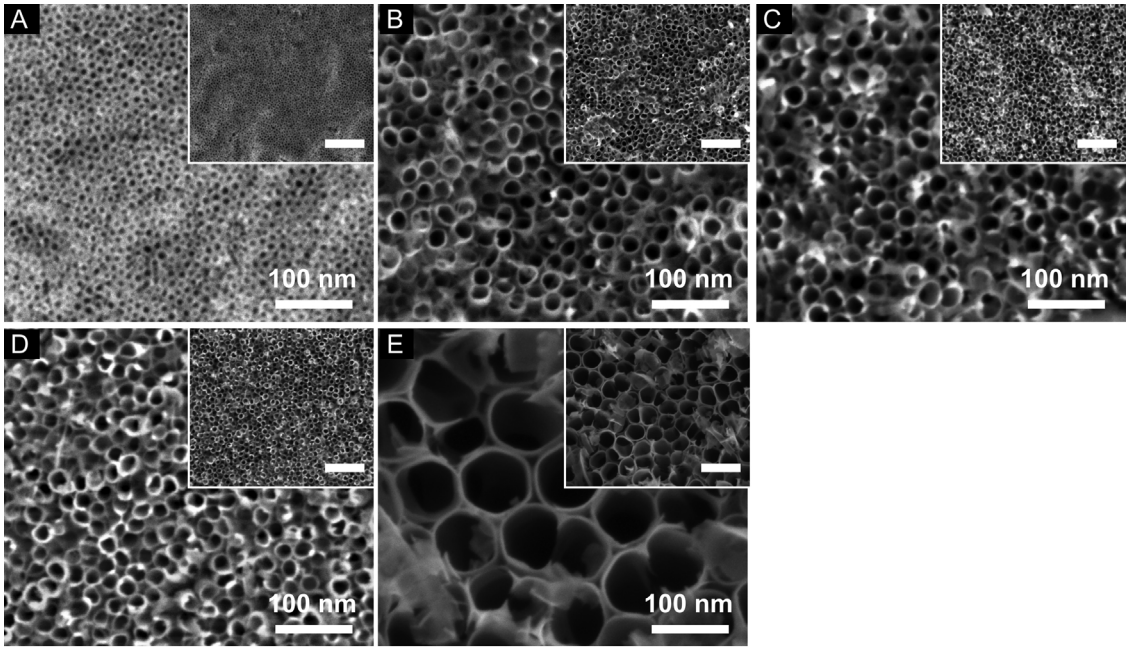

Fig. 3 – Titanium anodized surfaces at (A) 5 V, (B) 15 V, (C) 25 V, (D) 45 V, and (E) 60 V. The inset in each figure present a lower magnification micrograph and its scale bar represent 300 nm.

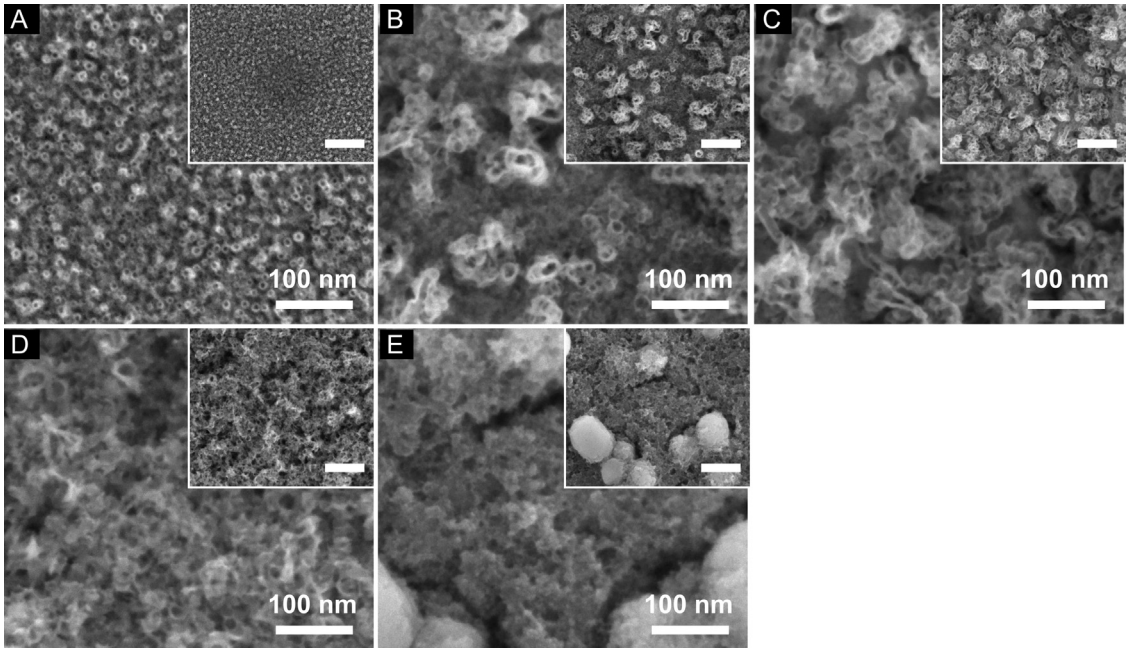

Fig. 4 – TiNi anodized surfaces at (A) 5 V, (B) 15 V, (C)25 V, (D) 45 V, and (E) 60 V. The inset in each figure present a lower magnification micrograph and its scale bar represent 300 nm.

of the electronic current is related to the nanotube diameter. The same behavior was found for TiNi samples, where tubular-shaped structures were found at the potentials of 5, 15, and 25 V, but the typical rise of total anodization current was not observed, even though nanotubular structures were produced, as shown in Fig. 4.

TiNi alloy *i x t* curves in Fig. 2(B) have similar behavior for anodization potentials of 5, 15, and 25 V, but a sharp current rise was found for both 15 and 25 V samples after approximately 3000 s. Anodization at 45 and 60 V reached much higher current densities after 30 s, with a similar pattern to the results of Yang et al. [39] for anodization under breakdown conditions of titanium. The rise of total current can be associated with the intense oxygen gas evolution during the anodization process, except for the 5 V sample where it was not detected. The sponge-like oxide nanostructures shown in Fig. 4(B, C, D, and E) are associated with the intense gas evolution as previously reported [39,40]. The higher current densities observed are in accordance with previous results that showed higher reaction rates for anodic processes in TiNi alloys [30]. The fact that the β phase showed higher dissolution rates in dual-phase α/β Ti-Al-V alloys [12,15,23,24] during anodization to obtain nanotubular surfaces was always attributed to the fact that β stabilizer V alloying elements increase its reactiveness. A recent study also found supporting evidence that anodic TNT's growth in a fully β Ti-50Nb proceeds at higher reaction rates compared to α containing alloys [41]. The same result obtained with fully β alloy suggests that the crystal structure of the substrate may be a contributing reason for differentiated reaction rates since the alloying elements are different.

In Fig. 4(A) it is possible to see that at 5 V anodization potential well-defined nanotubes are formed on top of TiNi alloy, but these nanotubes showed a lower degree of organization when compared to the same anodization conditions of cp-Ti. As the anodization potential increases, the level of self-organization obtained at 5 V completely disappears and a disordered nanoporous anodic film is obtained. In Fig. 4(B) it is possible to resolve some tubular structures dispersed in a matrix of sponge-like oxide structure at anodization potential of 15 V. The disorder degree increases when the potential increase to 25 V in Fig. 4(C), nevertheless some structures with tube-like shapes can be noticed. At anodization potentials of 45 and 60 V, all tubular structures are lost and only a sponge-like anodic film is obtained. The increase in disorder of the nanostructures and the transition from nanotubular to sponge-like oxide as the anodization potential increased is related to intense gas evolution at the anion contaminated layer and barrier oxide interface [34,39]. TiNi samples anodized at 45 and 60 V show overall aspects of pitting corrosion when *i x t* current density curves in the inset of Fig. 2(B) are analyzed, together with the surface analysis presented in Fig. 5. In fact, in their study Oliveira et al. [42] discuss the difficulties to grow titania nanotube arrays on top of a fully β Ti-15Mo alloy and, to achieve this objective, the anodization is performed in a water-free electrolyte with low NH_4F concentration and high anodization potential. These conditions refer to milder processes, once the electrolytes with higher water content affect directly the level of self-organization and enhance the chemical dissolution rate of oxides. However, a minimum H_2O content is necessary to produce TNT's, because water hydrolysis is the main source of oxygen ions to proceed with oxide growth and gaseous oxygen evolution [13].

When the total anodization current curves are analyzed for TiNi samples, one can notice that, after approximately 3000 s, there is a current raise for samples obtained at 15 and 25 V. This behavior may be related to the degeneration of the nanotubu-

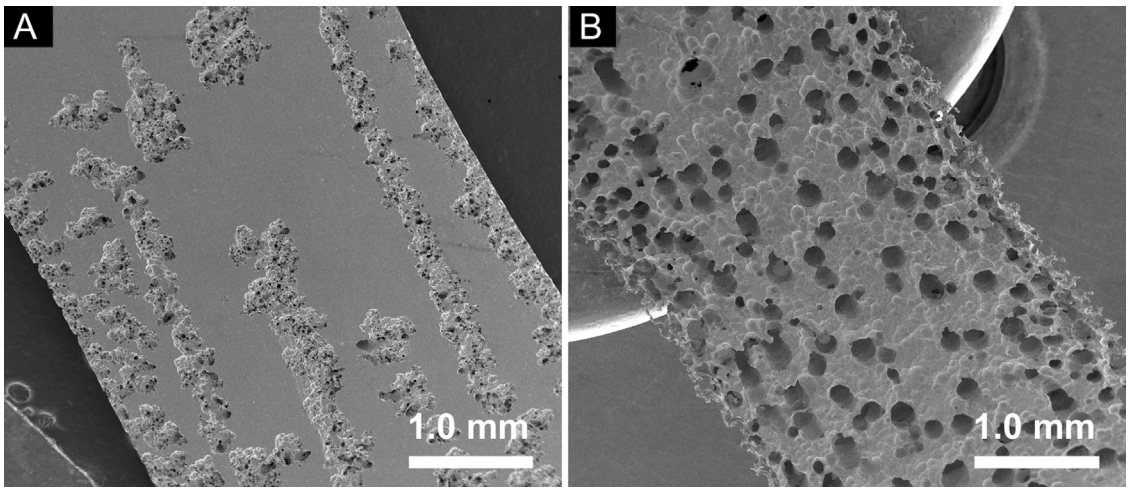

Fig. 5 – Surface aspects of TiNi strips anodized at potentials of (A) 45 V and (B) 60 V.

lar structure and, in order to investigate this effect, another anodization batch was performed at 5, 15 and 25 V with a total time of 2700s. The total anodization current plots and the surfaces of these samples are presented in Fig. 6. It can be noticed that total anodization current, shown in Fig. 6(A), is similar to what was found at 2700s in the first anodization batch. Well defined nanotubes, evenly spread through the surface, were obtained at anodization at 5 V. The other two conditions lead to nanotube formation at isolated particles dispersed in a matrix of porous oxide, suggesting that the process reached breakdown conditions even though no sharp current rise was found at the total current plot. The nanotubular formations are shown in Fig. 6 (B, C, and D) and the isolated particles at the insets. Also, it is possible to notice that the structure of the tubes is increasingly deteriorated as the anodizing potential increases. The water content for TNT's growth on the cp-Ti

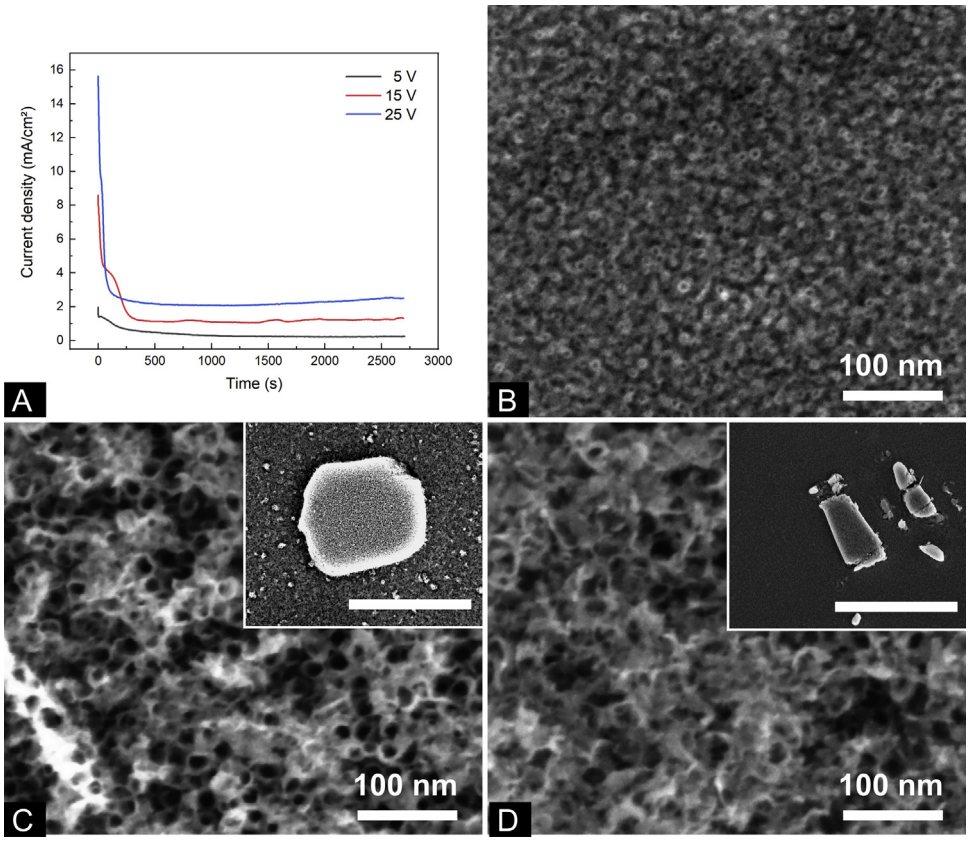

Fig. 6 – (A) Current density vs time plot of anodization at 5, 15, and 25 V. (B), (C), and (D) depicts the morphology of the anodic films obtained at 5, 15, and 25 V, respectively. Insets show the particles where the images were acquired and the scale bar of (C) and (D) insets represent 3 μm and 10 μm, respectively.

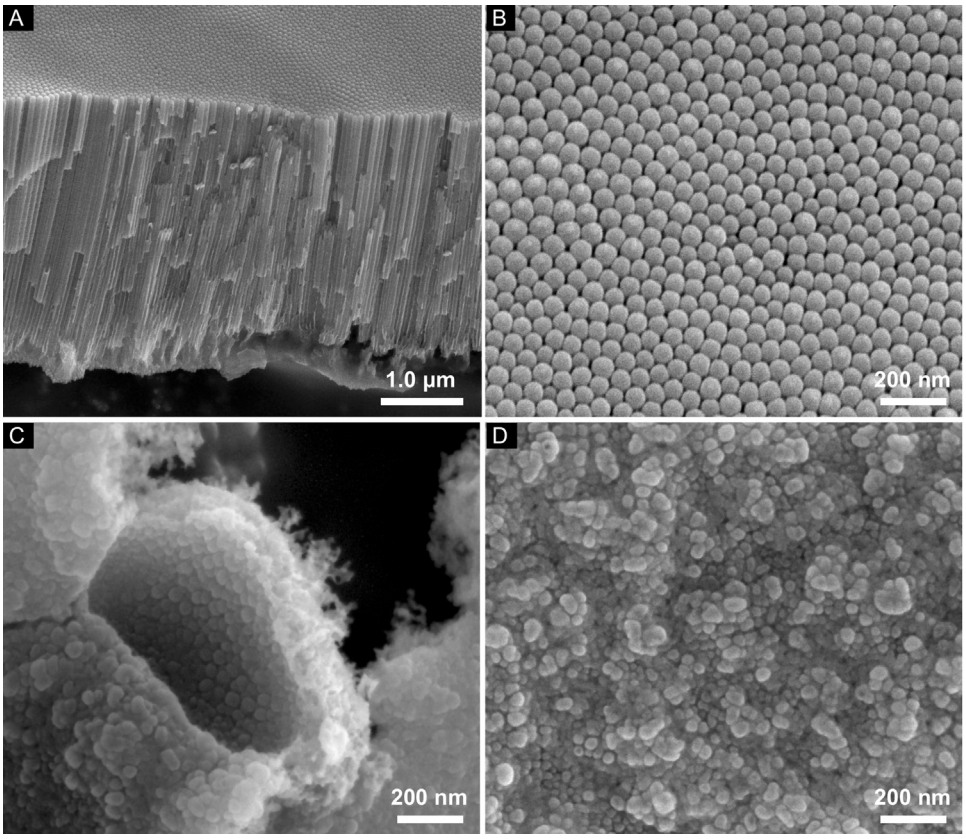

Fig. 7 – (A) Sideview and (B) bottom view of titania TNT's obtained at the cp-Ti substrate. (C) Sideview and (D) bottom view of the anodic film obtained at the TiNi substrate. Both materials were anodized at 25 V.

ranged between 1 and 5 %v. [13]; however, our results show that due to the higher reactiveness of the TiNi alloy, a suitable condition for nanotubes growth in titanium is too aggressive for TiNi anodization. These results differ from the ones obtained by Gao et al. [26], in which the optimal water contents were in the range of 0.5 and 1%v. The fact that lower anodization potential was capable to produce titania nanotubes in TiNi is also strong evidence of this behavior.

Fig. 7 shows the side and the bottom views of the nanotubes anodized at 25 V. Vertically aligned nanotubes with smooth walls were obtained for titanium anodization (Fig. 7(A)), with hemispherical morphology in each tube bottom at the metal/oxide interface (Fig. 7(B)). Also, the nature of the self-organization of titania nanotubes growth is noticeable, since it is possible to see clusters of hexagonally organized NT's. Oppositely, the anodic film formed at the TiNi surface, Fig. 7(C), does not possess vertically aligned tubes, even though some tube formation is seen at the surface of the films. Besides that, hemispherical formation at metal/oxide interfaces is present in Fig. 7(D), but they do not show auto organization features in their morphology. The specific formation of hemispherical nanotube bottom was investigated by Liao et al. [35] on anodization in oxalic acid and ammonium fluoride mixed electrolytes. For a given composition of NH_4F on oxalic electrolyte, a transient state was associated with the existence of an electronic current component where compact oxide is formed together with nanotube embryos [35]. The mechanism of tube nucleation and growth from O_2 generation at the anion contaminated and barrier oxide layers interface leads to the formation of the morphological features of the oxide at this interface [34,35]. Therefore, the formation of disorganized hemispherical shapes at the metal/oxide interface of TiNi, Fig. 7(D), endorses the hypothesis that nanotube forma-

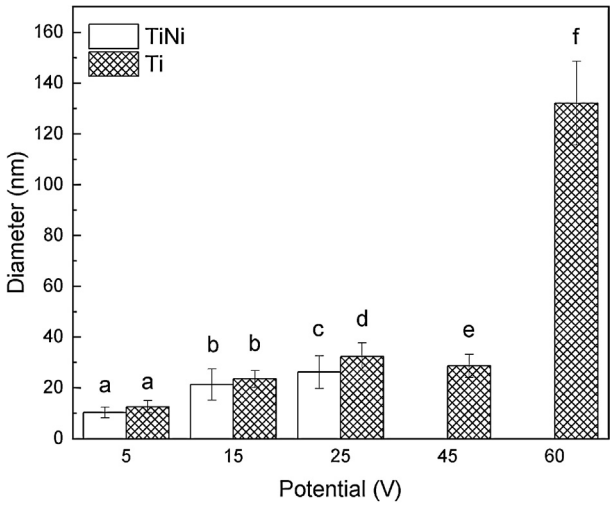

Fig. 8 – Bar plot of nanotubes diameter and their associated standard deviation. Different superscript letters mean significant differences at a confidence level of 0.95.

tion takes place at some level during anodic processing, but the products are degraded by intense oxygen evolution. The anodic film thickness of anodized titanium has $3.23 \pm 0.34\ \mu m$, whilst the film in TiNi is only $0.153 \pm 0.017\ \mu m$ thick, disclosing the higher reaction rates of TiNi substrates.

The adjusted analysis of variance model considering the individual effect of anodization potential and substrate type, and the mixed effects of both variables, lead to a conclusion that all variables may contribute to the differences found amongst the groups with $p < 0.05$. Pairwise comparisons were performed using Tukey's honestly significant differences and the conclusions are presented in Fig. 8. All groups of anodization potentials, except for 25 V, showed no significant differences between the diameter for both substrates. Also, a peak diameter was found for anodization at 25 V, similar to what as previously found by Gao et al. [26].

4. Conclusions

In the present work, we performed a comparative study between electrochemical anodization of commercially pure titanium and TiNi strips aiming the production of titania nanotubes structured surfaces. The resulting anodic film morphological characteristics were assessed and compared regarding tube morphology and the electrochemical process itself. Both cp-Ti and TiNi substrates were found to be monophasic and were constituted by α-Ti and β TiNi, respectively.

The anodization of cp-Ti resulted in nanotubular structures at all the evaluated conditions. The tubes presented diameters in the range of 10–30 nm, except for the anodization at 60 V that resulted in nanotubes around 130 nm in diameter. For TiNi substrate, well defined, and less organized than its Ti correspondent, nanotubular arrays were produced at an anodization potential of 5 V. As the potential increased a transition from TNT's to sponge-like oxide.The morphology observed by FE-SEM could be correlated with *i x t* curves, indicating that the involved anodic processes occurred at higher rates for the TiNi substrate when compared to cp-Ti for the same potential. The TiNi samples that were anodized for 2700s showed that TNT's were formed in isolated particles dispersed in a matrix of sponge-like oxide due to oxygen evolution.

The metal/oxide interface analysis showed that hemispherical nanotube bottoms are formed for cp-Ti anodization with a high level of self-organization. Also, it was possible to see a clear vertical alignment of nanotubes with a thickness of 3.23 μm. For TiNi samples, the cross-section view shows an oxide layer formation with a thickness of 0.153 μm and no vertical alignment. However, at the metal/oxide interface, it was possible to differentiate hemispherical formation, pointing to the same mechanism of oxide growth based on the oxygen bubble mold theory, but with a significantly lower organization degree. The presence of similar mechanisms of pore initiation, together with lower thickness leads to a conclusion that the nanotubular formation was initiated but the severity of the anodic process at higher potentials promoted the degradation of the nanostructured surface.

Conflict of interest

The authors declare no conflicts of interest.

Acknowledgment

This work was financed by Coordenação de Aperfeiçoamento de Pessoal de Nível Superior – Brasil (Capes) – Finance Code 001, Conselho Nacional de Desenvolvimento Científico e Tecnológico – Brasil (CNPq), Fundação de Amparo à Pesquisa do Estado de Minas Gerais – Brasil (Fapemig) and Pró-Reitoria de Pesquisa da Universidade Federal de Minas Gerais (PRPq/UFMG). The authors acknowledge the Center of Microscopy at the Universidade Federal de Minas Gerais (http://www.microscopia.ufmg.br) for providing the equipment and technical support for experiments involving electron microscopy.

REFERENCES

[1] Sidambe AT. Biocompatibility of advanced manufactured titanium implants-A review. Materials (Basel) 2014;7:8168–88, http://dx.doi.org/10.3390/ma7128168.
[2] Peters M, Kumpfert J, Ward CH, Leyens C. Titanium alloys for aerospace applications. Adv Eng Mater 2003;5:419–27, http://dx.doi.org/10.1002/adem.200310095.
[3] Zhang T, Liu Y, Zhang F, Xiao X. Polylysine-modified titania nanotube arrays for local drug delivery. Micro Nano Lett 2018;13:93–5, http://dx.doi.org/10.1049/mnl.2017.0312.
[4] Damodaran VB, Bhatnagar D, Leszczak V, Popat KC. Titania nanostructures: a biomedical perspective. RSC Adv 2015;5:37149–71, http://dx.doi.org/10.1039/c5ra04271b.
[5] Losic D, Aw MS, Santos A, Gulati K, Bariana M. Titania nanotube arrays for local drug delivery: recent advances and perspectives. Expert Opin Drug Deliv 2015;12:103–27, http://dx.doi.org/10.1517/17425247.2014.945418.
[6] Shen S, Chen J, Wang M, Sheng X, Chen X, Feng X, et al. Titanium dioxide nanostructures for photoelectrochemical applications. Prog Mater Sci 2018;98:299–385, http://dx.doi.org/10.1016/j.pmatsci.2018.07.006.
[7] Peighambardoust NS, Khameneh Asl S, Mohammadpour R, Asl SK. Band-gap narrowing and electrochemical properties in N-doped and reduced anodic TiO2 nanotube arrays. Electrochim Acta 2018;270:245–55, http://dx.doi.org/10.1016/j.electacta.2018.03.091.
[8] Lin LY, Yeh MH, Tsai KW, Chen CY, Wu CG, Ho KC. Highly ordered TiO2 nanotube stamps on Ti foils: synthesis and application for all flexible dye-sensitized solar cells. Electrochem commun 2013;37:71–5, http://dx.doi.org/10.1016/j.elecom.2013.10.011.
[9] Yoo H, Kim M, Kim Y-T, Lee K, Choi J. Catalyst-doped anodic TiO2 nanotubes: binder-free electrodes for (photo) electrochemical reactions. Catalysts 2018;8:555, http://dx.doi.org/10.3390/catal8110555.
[10] Kumar N, Chauhan NS, Mittal A, Sharma S. TiO 2 and its composites as promising biomaterials: a review. BioMetals 2018;31:147–59, http://dx.doi.org/10.1007/s10534-018-0078-6.
[11] Gong D, Grimes CA, Varghese OK, Hu W, Singh RS, et al. Titanium oxide nanotube arrays prepared by anodic oxidation. J Mater Res 2001;16:3331–4, http://dx.doi.org/10.1557/JMR.2001.0457.
[12] Zwilling V, Darque-Ceretti E, Boutry-Forveille A, David D, Perrin MY, Aucouturier M. Structure and physicochemistry of

anodic oxide films on titanium and TA6V alloy. Surf Interface Anal 1999;27:629–37, http://dx.doi.org/10.1002/(SICI)1096-9918(199907)27:7<629::AID-SIA551>3.0.CO;2-0.
[13] Fu Y, Mo A. A review on the electrochemically self-organized titania nanotube arrays: synthesis, modifications, and biomedical applications. Nanoscale Res Lett 2018;13, http://dx.doi.org/10.1186/s11671-018-2597-z.
[14] Regonini D, Bowen CR, Jaroenworaluck A, Stevens R. A review of growth mechanism, structure and crystallinity of anodized TiO2 nanotubes. Mater Sci Eng R Rep 2013;74:377–406, http://dx.doi.org/10.1016/j.mser.2013.10.001.
[15] Lee K, Choe HC, Ko YM, Brentley WA. Nanotubular structure formation on Ti-6A1-4V and Ti-Ta alloy surfaces by electrochemical methods. J Korean Inst Met Mater 2012;50:164–70, http://dx.doi.org/10.3365/KJMM.2012.50.2.164.
[16] Lu K, Tian Z, Geldmeier JA. Polishing effect on anodic titania nanotube formation. Electrochim Acta 2011;56:6014–20, http://dx.doi.org/10.1016/j.electacta.2011.04.098.
[17] Lin T, Liao M, Zhao S, Fan H, Zhu X. Anodic TiO2nanotubes produced under atmospheric pressure and in vacuum conditions. Ceram Int 2018;44:1764–70, http://dx.doi.org/10.1016/j.ceramint.2017.10.109.
[18] Huo S, Xu Z, Yin M, Yu D, Chen X, Wang H, et al. Improved growth rate of anodized TiO2nanotube arrays under reduced pressure field and light illumination. Sci Bull (Beijing) 2017;62:332–8, http://dx.doi.org/10.1016/j.scib.2017.01.036.
[19] Asgari V, Noormohammadi M, Ramazani A, Kashi MA. A facile method to form highly-ordered TiO2 nanotubes at a stable growth rate of 1000 nm min-1 under 60 v using an organic electrolyte for improved photovoltaic properties. J Phys D Appl Phys 2017;50, http://dx.doi.org/10.1088/1361-6463/aa812a.
[20] Albu SP, Ghicov A, Macak JM, Schmuki P. 250 μm long anodic TiO2 nanotubes with hexagonal self-ordering. Phys Status Solidi - Rapid Res Lett 2007;1:65–7, http://dx.doi.org/10.1002/pssr.200600069.
[21] Zhou X, Nguyen NT, Özkan S, Schmuki P. Anodic TiO2 nanotube layers: why does self-organized growth occur—a mini review. Electrochem commun 2014;46:157–62, http://dx.doi.org/10.1016/j.elecom.2014.06.021.
[22] Lockman Z, Sreekantan S, Ismail S, Schmidt-Mende L, MacManus-Driscoll JL. Influence of anodisation voltage on the dimension of titania nanotubes. J Alloys Compd 2010;503:359–64, http://dx.doi.org/10.1016/j.jallcom.2009.12.093.
[23] Matykina E, Conde A, de Damborenea J, Marero DMY, Arenas MA. Growth of TiO2-based nanotubes on Ti–6Al–4V alloy. Electrochim Acta 2011;56:9209–18, http://dx.doi.org/10.1016/j.electacta.2011.07.131.
[24] Moravec H, Vandrovcova M, Chotova K, Fojt J, Pruchova E, Joska L, et al. Cell interaction with modified nanotubes formed on titanium alloy Ti-6Al-4V. Mater Sci Eng C 2016;65:313–22, http://dx.doi.org/10.1016/j.msec.2016.04.037.
[25] Otsuka K, Ren X. Physical metallurgy of Ti–Ni-based shape memory alloys. Prog Mater Sci 2005;50:511–678, http://dx.doi.org/10.1016/j.pmatsci.2004.10.001.
[26] Hang R, Liu Y, Zhao L, Gao A, Bai L, Huang X, et al. Fabrication of Ni-Ti-O nanotube arrays by anodization of NiTi alloy and their potential applications. Sci Rep 2015;4:7547, http://dx.doi.org/10.1038/srep07547.
[27] Hang R, Liu Y, Gao A, Bai L, Huang X, Zhang X, et al. Highly ordered Ni-Ti-O nanotubes for non-enzymatic glucose detection. Mater Sci Eng C 2015;51:37–42, http://dx.doi.org/10.1016/j.msec.2015.02.027.
[28] Liu Y, Ren Z, Bai L, Zong M, Gao A, Hang R, et al. Relationship between Ni release and cytocompatibility of Ni-Ti-O nanotubes prepared on biomedical NiTi alloy. Corros Sci 2017;123:209–16, http://dx.doi.org/10.1016/j.corsci.2017.05.006.
[29] Hang R, Liu Y, Bai L, Zong M, Wang X, Zhang X, et al. Electrochemical synthesis, corrosion behavior and cytocompatibility of Ni-Ti-O nanopores on NiTi alloy. Mater Lett 2017;202:5–8, http://dx.doi.org/10.1016/j.matlet.2017.05.089.
[30] Hang R, Liu Y, Liu S, Bai L, Gao A, Zhang X, et al. Size-dependent corrosion behavior and cytocompatibility of Ni-Ti-O nanotubes prepared by anodization of biomedical NiTi alloy. Corros Sci 2015;103:173–80, http://dx.doi.org/10.1016/j.corsci.2015.11.016.
[31] Schneider CA, Rasband WS, Eliceiri KW. NIH Image to ImageJ: 25 years of image analysis. Nat Methods 2012;9:671–5, http://dx.doi.org/10.1038/nmeth.2089.
[32] R Core Team. R: a language and environment for statistical computing; 2018.
[33] Roy P, Berger S, Schmuki P. TiO2 nanotubes: synthesis and applications. Angew Chemie Int Ed 2011;50:2904–39, http://dx.doi.org/10.1002/anie.201001374.
[34] Zhou Q, Tian M, Ying Z, Dan Y, Tang F, Zhang J, et al. Dense films formed during Ti anodization in NH4F electrolyte: evidence against the field-assisted dissolution reactions of fluoride ions. Electrochem commun 2020;111:106663, http://dx.doi.org/10.1016/j.elecom.2020.106663.
[35] Liao M, Ma H, Yu D, Han H, Xu X, Zhu X. Formation mechanism of anodic titanium oxide in mixed electrolytes. Mater Res Bull 2017;95:539–45, http://dx.doi.org/10.1016/j.materresbull.2017.08.041.
[36] Jin R, Liao M, Lin T, Zhang S, Shen X, Song Y, et al. Formation and evolution of anodic TiO 2 nanotube embryos. Mater Res Express 2017;4:065008, http://dx.doi.org/10.1088/2053-1591/aa72b1.
[37] Zhao S, Li C, Wei T, Li C, Yu M, Cui H, et al. A mathematical model for initiation and growth of anodic titania nanotube embryos under compact oxide layer. Electrochem commun 2018;91:60–5, http://dx.doi.org/10.1016/j.elecom.2018.05.004.
[38] Shabalovskaya SA, Rondelli GC, Undisz AL, Anderegg JW, Burleigh TD, Rettenmayr ME. The electrochemical characteristics of native Nitinol surfaces. Biomaterials 2009;30:3662–71, http://dx.doi.org/10.1016/j.biomaterials.2009.03.034.
[39] Yang F, Feng X, Ge F, Zhang T, Qi J, Li D, et al. Rapid growth of titanium oxide nanotubes under the critical breakdown voltage: evidence against the dissolution reaction of fluoride ions. Electrochem commun 2019;103:17–21, http://dx.doi.org/10.1016/j.elecom.2019.04.010.
[40] Huang W, Xu H, Ying Z, Dan Y, Zhou Q, Zhang J, et al. Split TiO2 nanotubes – evidence of oxygen evolution during Ti anodization. Electrochem commun 2019;106:106532, http://dx.doi.org/10.1016/j.elecom.2019.106532.
[41] Chernozem RV, Surmeneva MA, Ignatov VP, Peltek OO, Goncharenko AA, Muslimov AR, et al. Comprehensive characterization of titania nanotubes fabricated on Ti-Nb alloys: surface topography, structure, physicomechanical behavior, and a cell culture assay. ACS Biomater Sci Eng 2020;6:1487–99, http://dx.doi.org/10.1021/acsbiomaterials.9b01857.
[42] Oliveira NTC, Verdério JF, Bolfarini C. Obtaining self-organized nanotubes on biomedical Ti-Mo alloys. Electrochem commun 2013;35:139–41, http://dx.doi.org/10.1016/j.elecom.2013.08.019.